

# Insight into the Effects of Water on the Ethene to Aromatics Reaction with HZSM-5

Huiqiu Wang, Yilin Hou, Wenjing Sun, Qikun Hu, Hao Xiong, Tiefeng Wang, Binhang Yan, and Weizhong Qian\*



Cite This: ACS Catal. 2020, 10, 5288–5298



Read Online

ACCESS |

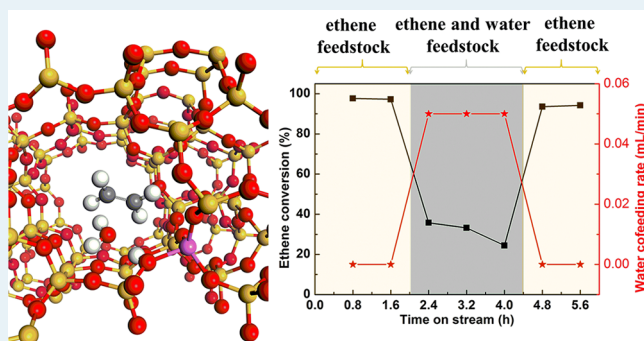
Metrics & More

Article Recommendations

Supporting Information

**ABSTRACT:** We report the effect of water on the conversion of ethene with H-ZSM-5 to make aromatics at 300–500 °C. We found that water seriously decreased the conversion of ethene and the yield of aromatics, suppressed the hydrogen transfer reaction, and changed the distribution of aromatics at low reaction temperature (300 °C). However, the effect of water became relatively insignificant with an increase in the reaction temperature. Characterization by TGA, *in situ* FTIR, and GC-MS and a simulation with DFT validated that the cofed water preferentially adsorbs at the Brønsted acid site (BAS) of the H-ZSM-5 catalysts, in comparison to ethene, leading to the formation of Z–OH···H<sub>2</sub>O hydrogen-bonded complexes and H<sup>+</sup>(H<sub>2</sub>O)<sub>n</sub> species. These species inside the channel of the zeolite inhibit the oligomerization of ethene, the olefin-induced hydrogen transfer reaction, and running of the hydrocarbon pool inside zeolite channels. We also validated that the conversion of ethene was recovered when the majority of H<sub>2</sub>O was desorbed from BAS, while the propagation of the HCP mechanism within HZSM-5 was still altered at higher temperature as a result of a physically adsorbed water-enhanced confinement effect in the channels. In addition, the role of water on the suppression of the amount of coke was investigated in detail.

**KEYWORDS:** ethene to aromatics, HZSM-5, water, Brønsted acid sites, HCP mechanism, coke



## INTRODUCTION

The conversion of oxygen-containing C<sub>1</sub> compounds (e.g., CH<sub>3</sub>OH, CO, and CO<sub>2</sub>) into aromatics with zeolites having acidic sites is a very important catalytic route for the upgrading of coal and biomass.<sup>1–12</sup> Water and low-carbon-number hydrocarbons are always the products or intermediate products by a dehydration reaction and a C–C bond formation reaction over the Brønsted acid sites (abbreviated as BASs) and Lewis acid sites (abbreviated as LASs) on the zeolite.<sup>2,13</sup> Further conversion of low-carbon-number hydrocarbons is necessary to form aromatics inside the zeolite in the presence of water. The competitive adsorption of water and hydrocarbons over the zeolite exhibits a certain influence on the conversion of reactants and the selectivity and yield of products. For instance, the selectivity to olefins was increased and the deactivation of the catalyst was decreased by adding water in the process of methanol to olefins (abbreviated as MTO).<sup>14</sup> Simulations suggested that competitive adsorption of water, methanol, and propene on BAS, giving a longer induction period in the MTO process.<sup>15</sup> For the activation of the C–H bonds of alkanes, a low loading of water ( $\leq 1$  water molecule per BAS) increased the reaction rate significantly, but higher loadings of water (about 2–3 water molecules per active site) retarded the reaction.<sup>16</sup> Similarly, for the dehydration of 1-

propanol<sup>17</sup> and the alkylation reaction of phenol with ethanol,<sup>18</sup> the adsorption states of reactants on the zeolite were influenced by water, resulting in a slow reaction rate. However, the dehydration of cyclohexanol was enhanced in an aqueous phase, due to the formation of hydronium ions confined in zeolite pores.<sup>19</sup> The activation energy of cyclohexene protonation at the hydronium ion was significantly higher than that at the framework-bound proton (BAS).<sup>20</sup> Generally, the transformation reactions of all of the above are catalyzed by BASs, originating from the substitution of Si<sup>4+</sup> by Al<sup>3+</sup> in the framework.<sup>21</sup> The mechanistic details of reactions catalyzed by BASs have been intensively investigated.<sup>21–24</sup> However, the effect of water on the elementary steps of zeolite-catalyzed reactions is not fully understood to date, as the real structure of a BAS cannot be represented by a framework proton in the presence of water.

Received: December 24, 2019

Revised: April 7, 2020

Published: April 8, 2020



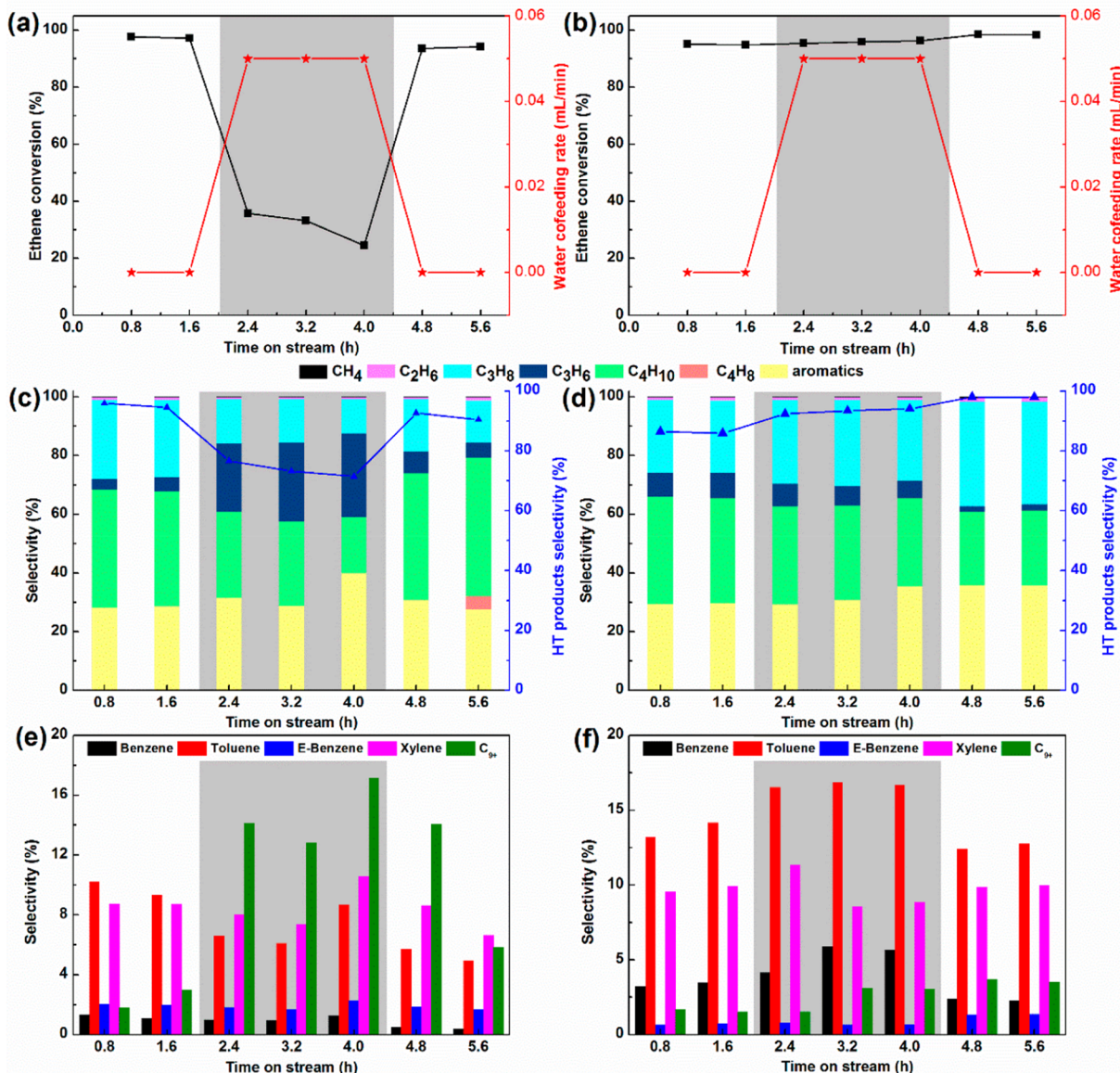


**Figure 1.** Effects of water cofeeding on the performance of H-ZSM-5 in the ethene conversion process: ethene conversion and water cofeeding rate at 300 °C (a) or 350 °C (b); products and hydrogen transfer product selectivities of the ethene conversion process at 300 °C (c) or 350 °C (d); aromatic product distributions of the ethene conversion process at 300 °C (e) or 350 °C (f). The shaded parts indicate the cofeeding of water during the ethene conversion process.

Herein, we attempted to study the effect of water on the conversion of ethene to aromatics with HZSM-5, a system similar to one of the consecutive steps in MTO or methanol to aromatics. The cofed water exhibited a significant effect on the conversion of ethene, the yield of aromatics, and the selectivity of byproducts at 300 °C but became insignificant at higher temperatures (350–450 °C). However, the cofed water exhibited very definite effects on the running of the HCP mechanism, the deposition of coke, and the presence of coke components at all reaction temperatures, as analyzed by TGA and GC-MS. An analysis with TGA, *in situ* FTIR, and density functional theory (DFT) suggested the competitive adsorption of water on a portion of the BASs and the formation of Z–OH···H<sub>2</sub>O hydrogen-bonded complexes and H<sup>+</sup>(H<sub>2</sub>O)<sub>n</sub> species at lower temperature. This resulted in the different densities and strengths of active BASs contributing to the formation of aromatics via hydrocarbon pool cycles, as well as

the hydrogen transfer reaction of olefins and dehydrogenation to produce coke at different temperatures. These results are useful to understand the effect of water on the heterogeneous catalytic conversion of olefin or methanol to aromatics over zeolites.

## EXPERIMENTAL METHOD

**Catalyst and Characterizations.** H-ZSM-5 (Si/Al ratio 12.5) was purchased from Nankai Catal. Corp., China. The sample was characterized by powder X-ray diffraction (XRD) with the use of a Rigaku D/Max-RB diffractometer, where the Cu K $\alpha$  radiation was set at 40 kV and 120 mA. The morphology of the sample (*Figure S1* in the Supporting Information) was characterized with a scanning electron microscope (SEM, JSM-7401), operated at 3.0 kV.

**In Situ FTIR and TGA Studies of the Desorption Process of Water over HZSM-5 Catalyst.** *In situ* FTIR

spectroscopy (Thermo Nicolet Nexus 470 spectrometer) was used to monitor the adsorption sites of  $\text{H}_2\text{O}$  on the zeolite. The zeolite sample was first heated to 100 °C in steam for 1 h to achieve a saturated adsorption and then cooled to ambient temperature. The sample powder was pressed onto a tungsten mesh with a K-type thermocouple attached and was transferred into the reaction chamber. Then the reaction chamber was integrated with the spectrometer and a highly sensitive detector of mercury cadmium telluride (MCT-A), which was cooled by liquid nitrogen. When the detection system was evacuated to  $1 \times 10^{-5}$  Pa, a baseline spectrum (resolution 4  $\text{cm}^{-1}$ ) was first recorded. For the gradual desorption of water, the sample was heated at a rate of 5 °C/min in 50 °C increments. The FTIR spectra were obtained when the sample was kept for 5 min at each targeted temperature.

Thermogravimetric analysis (TGA, TGA/DSC-1) was carried out from 30 to 650 °C at a rate of 10 °C/min in  $\text{N}_2$ . The water-preadsorbed sample was obtained in the same manner as above.

**IR Studies of the Coadsorption of Ethene and Water on HZSM-5 Catalyst.** The sample was pretreated in a quartz reactor with  $\text{N}_2$  at 500 °C for 60 min and then cooled to 100 °C. The sample was preadsorbed with different gases (steam and ethene) at 100 °C for 30 min. After the sample was pressed with KBr to be a sheet very quickly under dry conditions, the IR spectra of the sample were recorded at a resolution of 4  $\text{cm}^{-1}$ .

**TGA and GC-MS Studies of the Used HZSM-5 Catalyst Containing Coke.** The weight ratio of coke on the used HZSM-5 catalysts was analyzed by the same instrument above (TGA/DSC-1) from 30 to 800 °C at a heating rate of 10 °C/min in air.

For the analysis of coke with the GC-MS-QP2010 SE instrument, 0.3 g of the sample was dissolved in 3.0 mL of 50% HF solution. Then, the organics were extracted with 1.0 mL of  $\text{CH}_2\text{Cl}_2$ . After that, 0.2  $\mu\text{L}$  of the organics was analyzed by GC-MS with a Stabilwax-DA column, with an inner diameter of 0.25 mm, length of 60 m, and thickness of the stationary phase of 0.5  $\mu\text{m}$ . The temperature program in the analysis can be described as follows. First, the instrument was isothermally heated to 100 °C and kept constant for 20 min. Second, it was heated to 260 °C at a rate of 5 °C/min and kept constant at 260 °C for 15 min.

**Ethene to Aromatics (ETA) Conversion.** The ETA process was performed in a quartz packed-bed reactor (13.0 mm i.d.) with 0.5 g of the catalyst inside. The reactor was first heated to 550 °C under a nitrogen flow for 1 h to remove water or other species adsorbed on the catalyst. Then the reactor was cooled or heated to a desirable reaction temperature (300–500 °C) and ethene at a flow rate of 10 mL/min was fed in and converted at 1 atm. To study the effect of water, deionized water was injected at a flow rate of 0.03 mL/min by a dual microplunger pump. The as-produced hydrocarbons were detected with a gas chromatograph (GC-2014, equipped with two flame ionization detectors, Shimadzu Co.).

**DFT and GCMC Computational Method.** All periodic density functional theory (DFT) calculations were performed using the Vienna ab initio simulation package (VASP 5.4.5) with the projected augmented wave (PAW) formalism.<sup>25,26</sup> Key calculations with the functional, equations, and parameters are described in section SI-1 in the Supporting Information, following the suggestion of refs 27 and 28. In this work, H-

ZSM-5 zeolites are represented by a periodic 96T unit cell, which was obtained from a database of zeolite structures (<http://www.iza-structure.org/databases/>) (Figure S2 in the Supporting Information). The BAS was formed by a substituted aluminum atom (located at a T12 site in HZSM-5), and a charge-balancing proton was added on the most stable adjacent oxygen.

By definition, the adsorption energies of adsorbates on BAS in zeolites are determined by the formula

$$E_{\text{adsorption}} = E_{\text{Z-adsorbate}} - E_{\text{Z}} - E_{\text{adsorbate}} \quad (1)$$

where  $E_{\text{Z-adsorbate}}$ ,  $E_{\text{Z}}$ , and  $E_{\text{adsorbate}}$  are the electronic energies of the system after the adsorbate is adsorbed on the zeolite, the bare zeolite, and the adsorbate (g), respectively.

All of the grand canonical Monte Carlo (GCMC) simulations were performed using the Materials Studio simulation packages. The HMFI supercell used in GCMC simulations involves 8-unit cells ( $2 \times 2 \times 2$ ) of the MFI zeolite with a total of 767 Si atoms and one Al atom (located at the T12 site in one of the MFI unit cells). (Figure S3 in the Supporting Information) The detailed parameters for simulations are presented in section SI-2 in the Supporting Information.

## RESULTS AND DISCUSSION

**Effect of Water Cofeeding on the Performance of HZSM-5 in the ETA Process.** Figure 1a,c present the effects of water cofeeding on ETA over H-ZSM-5 catalyst at 300 and 350 °C. In the absence of water, the conversion of ethene is about 97.5% at 300 °C (0–2 h in Figure 1a) and the selectivities of propane, propene, and butane are close to 26%, 4%, and 40%, respectively. The selectivity of hydrogen transfer (HT) products in total, which includes propane and butane, is around 95%. However, the conversion of ethene was drastically decreased to 33% with the cofeeding of water (2–4.4 h in Figure 1a). The selectivities of propane and butane dropped to 14% and 28%, respectively. The selectivity of HT products in total dropped to 73% significantly. Meanwhile, the selectivity of propene increased drastically from 4% to 26%. After the feeding of water was stopped at 4.8–5.6 h, the conversion of ethene quickly recovered to 92%. The selectivity of propane, propene, butane, and HT products in total was recovered simultaneously. These results suggested that water adsorbed on the zeolite at 300 °C occupied BASs in large amounts, suppressing hydrogen transfer and the conversion of ethene.

Actually, ETA inside zeolite channels follows the hydrocarbon pool mechanism similarly to that for the transformation of methanol.<sup>1,29,30</sup>  $\text{C}_3$  species can be considered as the product of a dual cycle of aromatics pool and olefins pool, while the  $\text{C}_2$  species probably originated from both the reactants and the hydrocarbon pool. Actually, the product distributions of aromatics varied with the cofeeding of water. The selectivity to toluene (T) and xylene (X) both decreased significantly with the feeding of water at 2–4.4 h (Figure 1e). The selectivities of benzene (B) and ethylbenzene (EB) remained nearly the same, but the selectivity to  $\text{C}_{9+}$  remarkably increased from ~2% to ~14%. Actually, the 10-membered-ring pores of H-ZSM-5 are around  $5.3 \times 5.6$  Å, exhibiting shape selectivity for large molecules such as ortho and meta X (*o*-X and *m*-X) and  $\text{C}_{9+}$  and allowing only small molecules, including  $\text{C}_1$ – $\text{C}_5$  hydrocarbons, B, T, and PX, to diffuse out easily.<sup>5,31</sup> B, T, and X were the dominant products of the hydrocarbon pool of ZSM-5. The shape selectivity of ZSM-5 with medium pores

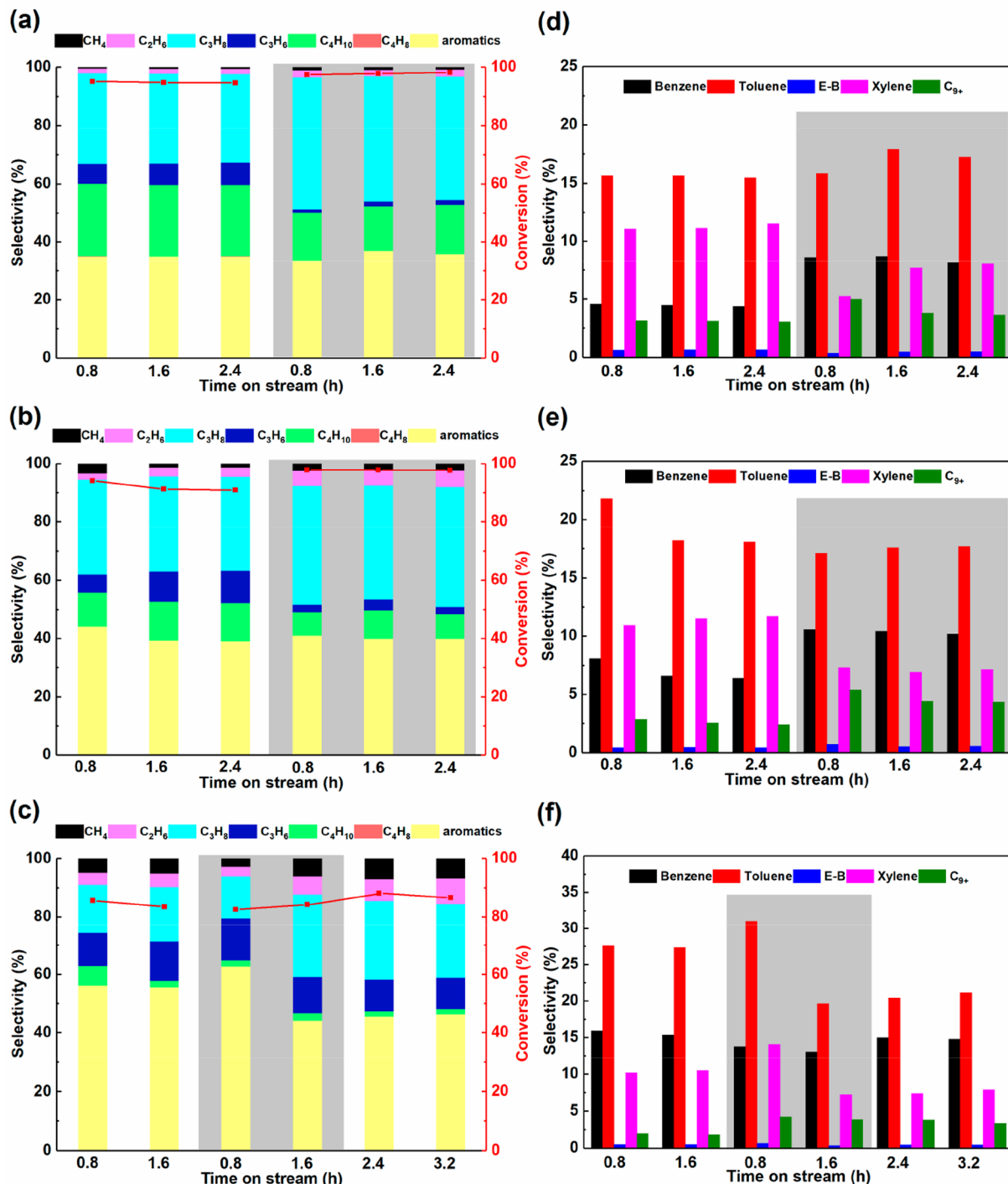


**Figure 2.** Effects of water cofeeding on the performance of H-ZSM-5 in the ETA process: ethene conversion and product selectivity at 400 °C (a), 450 °C (b), and 500 °C (c); aromatic product distributions of the ethene conversion process at 400 °C (d), 450 °C (e), and 500 °C (f). The shaded parts indicate the cofeeding of water during the ethene conversion process.

resulted in a low yield of EB, which was produced only via the isomerization of X and alkylation on the external surface or at the pore mouth. C<sub>9+</sub> is mainly produced by the alkylation of ethene with T or X. Similar, switching off the water at 4.8–5.6 h resulted in the quick decrease in the selectivity of C<sub>9+</sub>. These results further validated that the interaction of water with BASs inside the zeolite channel exerted a significant effect on the hydrocarbon pool, by tuning the density of BASs and the space confinement effects inside the channel.

In addition, the performance of H-ZSM-5 in the ETA process was investigated at 350 °C with and without cofeeding of water. Less change in ethene conversion and product selectivity can be discerned, validating that water cofeeding has no effect on the ethene conversion process at 350 °C (Figure 1b,d,f). Increasing the temperature from 300 to 350 °C resulted in a significant increase in the selectivities of B, T, and X and the rapid decrease in the selectivities of EB and C<sub>9+</sub>. These directly validated the easy desorption of water from

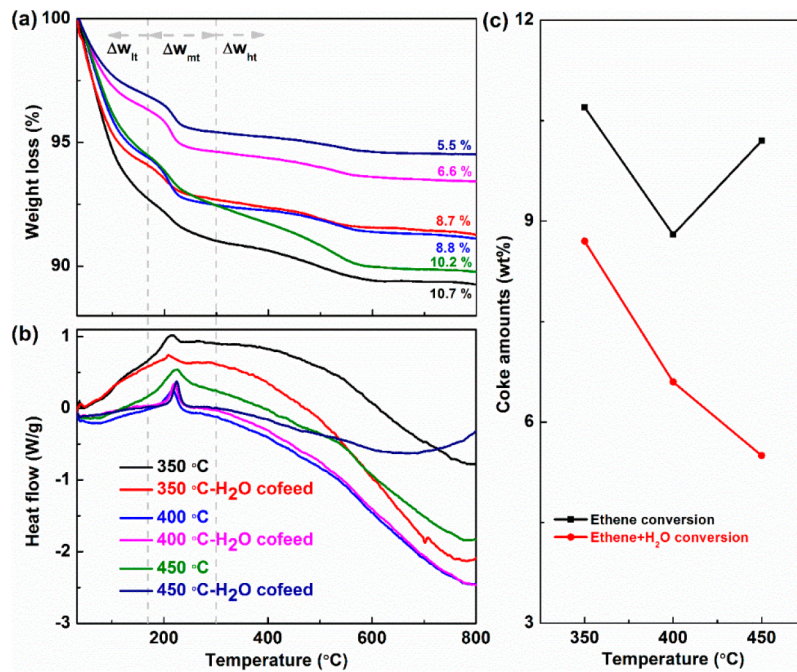


**Figure 3.** Comparison of the effects with and without addition of water: TGA curves (a), heat flow curves (b), and the coke amounts (c) of spent HZSM-5 after reactions at different temperatures with TOS = 4.5 h.

BASs with an increase in reaction temperature. This results in a large amount of BASs and sufficient space in the zeolite for the smooth building and running of the hydrocarbon pool. Therefore, alkylation reactions over the external surface of the zeolite, contributing to the formation of EB and C<sub>9+</sub>, became relatively insignificant.

As expected, the effect of cofeeding water on ETA over H-ZSM-5 became relatively insignificant at 400, 450, and 500 °C (Figure 2). The selectivities of ethane and propane increased with the cofeeding of water at 400–450 °C (Figure 2a,b), in comparison to those at 300–350 °C. The selectivity of butane was significantly decreased as water was added at 400–450 °C. The propene/propane ratios with water were much smaller than those without water at 400–450 °C, suggesting that the effect of water on the suppression of hydrogen transfer became weak. As an overall result, the total selectivity of aromatics remained nearly unchanged, probably due to the conversion of butane (to aromatics, ethane, and methane). However, the distributions of aromatics varied as water was added. The selectivities to B and C<sub>9+</sub> both increased, and the selectivity to X decreased (Figure 2d,e), in agreement with previous work that the formation of HCP species (e.g. *o*-X, *m*-X, and trimethylbenzene (TriMB)) can be tuned with water.<sup>15</sup> In addition, the conversion of ethene at 500 °C decreased by 5–10% with or without addition of water (Figure 2c), mainly due to the deposition of coke. Apparently, the deposition of coke weakened the BASs for the hydrogen transfer reaction, giving a higher yield of propene again. The yields of T and X decreased, but the yield of TriMB (C<sub>9+</sub>) increased at 500 °C (Figure 2f). The total yield of aromatics increased by 5–8% at 0.8 h as water was added, in comparison to that without addition of water (Figure 2c).

**Effects of Cofeeding Water on the Formation of Coke and the Dual-Cycle Mechanism in the ETA Process.** TGA was employed to study the coke on the spent catalysts reacted from 350 to 450 °C (Figure 3a). Weight losses at low

temperature ( $\Delta w_{lt}$  at <175 °C), medium temperature ( $\Delta w_{mt}$  at 175–300 °C) and high temperature ( $\Delta w_{ht}$  at >300 °C) are attributed to the desorption of volatile compounds and the combustion of “soft coke” compounds and “hard coke” compounds, respectively (referred to as “MABs” and “PHAs”, respectively) (Table S1 in the Supporting Information).<sup>32,33</sup> The  $\Delta w_{lt}$  value at 350 °C exhibited a significant difference with or without addition of water. However, the associated values of heat flow are nearly the same (Figure 3b). This means that the low-volatility compounds produced in different processes are the same but the amounts are different. However, the  $\Delta w_{mt}$  value and heat flow are both different, suggesting the species of soft coke and their amounts are both different with and without feeding water at 350 °C. In contrast, with an increase in reaction temperature to 450 °C, we found the species of soft coke are nearly the same and are independent of whether or not water is added. In the reaction temperature range of 350–400 °C, the  $\Delta w_{lt}$  and  $\Delta w_{ht}$  values decreased from 7.3% to 5.7% and from 1.8% to 1.3%, respectively. These results validated again that water exhibited a significant effect on the process at lower reaction temperatures.

Very strangely, the coke amounts exhibited an inverted volcano-shaped variation trend as the reaction temperature was varied in the conversion of pure ethene (Figure 3c). The turning point occurred at 400 °C, probably due to the reversible alkylation of aromatics or the dealkylation of multimethylbenzene at 300–400 °C.<sup>34</sup> For the case of reaction at 450 °C, the  $\Delta w_{lt}$  value remained unchanged, whereas the  $\Delta w_{ht}$  value increased from 1.3% to 2.6%, due to the further dehydrogenation effect of soft coke to become hard coke. In comparison, the production of coke was apparently suppressed by the addition of water. The amount of coke decreased sustainably with an increase in reaction temperature from 300 to 450 °C (Figure 3c). In detail, the  $\Delta w_{mt}$  and  $\Delta w_{ht}$  values

decreased when water was added into the feedstock at 350–450 °C.

The coke on the spent catalysts was detected by GC-MS (Figure 4). The proportions and concentrations of these

exhibited different activities and selectivities toward the final products,<sup>43–45</sup> the change of their species by addition of water at temperatures of 350 °C or above resulted in the different distributions of aromatics, in comparison to those in dry ETA.

In general, the typical carbonaceous compounds in coke are primarily naphthalene and anthracene. The addition of water resulted in a significant decrease in the ratio of di- and tricyclic aromatics, associated with the changing trends in coke amounts (Figure 3). In addition, the species of coke can be classified into multialkylbenzenes (MABs) (i.e., triethylbenzene, 1,3-diethyl-5-methylbenzene, 1-ethyl-2,4,5-trimethylbenzene) and polycyclic aromatic hydrocarbons (PAHs). PAHs can be dominantly produced from the alkylated, single-ring aromatics in the methanol conversion process,<sup>46,47</sup> where water, ethene, and propylene are products or intermediates. In contrast, the formation of coke in the dry ETA process follows another pathway from polyolefins to PAHs (Scheme S1 in the Supporting Information).<sup>48</sup> Very recently, the use of operando UV–Raman spectroscopy validated that methylbenzenium carbenium ions ( $\text{MB}^+$ ) were key precursors for the formation of coke and that water can effectively prevent  $\text{MB}^+$ s from growing into PAHs.<sup>33</sup> Combining these results together, we propose that the addition of water did not influence the formation of MABs but suppressed the formation of PAHs from conjugated polyolefins and postponed the condensation and polymerization from  $\text{MAB}^+$ s to PAHs.

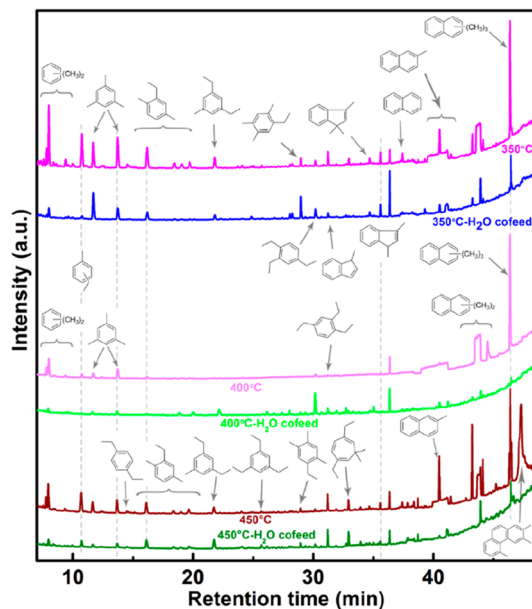


**Figure 4.** Temperature-dependent GC-MS pattern of organics extracted from the spent catalysts in the ETA process (TOS = 4.5 h), with and without cofeeding of water.

organic compounds, represented by the intensities of the GC-MS signals, distinctly changed on cofeeding of water. The amount of the predominant species of coke, such as methylbenzenes (MBs) (i.e., X, TriMB) and ethyltoluene, was significantly decreased with addition of water, validating the strong negative effect of water on the propagation of the aromatic-based cycle. Note that the carbenium ions act as the significant intermediates inside the zeolite.<sup>35–42</sup> To date, some carbenium ions, such as heptamethylbenzenium (heptaMB<sup>+</sup>) and methylcyclopentenyl (MCP<sup>+</sup>) cations, have been identified in H-beta zeolite with large pore mouths<sup>41</sup> and zeolites with small pore mouths but a large cage (i.e., SAPO-34, SSZ-13, and DNL-6).<sup>39,40,42</sup> In addition, 2,4,6-pentamethylbenzenium and 1,3-dimethylcyclopentenyl cations were found in H-ZSM-5 with medium pores.<sup>36,38</sup> Since different carbenium ions

**TGA and *In Situ* FTIR Spectroscopic Studies of the Desorption of Water from HZSM-5.** The amount of water remaining after desorption was quantitatively determined with TGA and normalized to the Al atom in H-ZSM-5 (Figure 5a). An obvious weight loss occurred at 30–100 °C, ascribed to the desorption of physically adsorbed water and the decoordination of water from the clusters of  $\text{H}^+(\text{H}_2\text{O})_n$ .<sup>49</sup> Quantitatively, the average  $\text{H}_2\text{O}/\text{Al}$  atom ratio is 26 at 30 °C, but the value decreased drastically to 2.6 at 100 °C. A further increase in temperature resulted in a gradual decrease in the amount of water inside H-ZSM-5 and the complete removal of water molecules at ~500 °C. Quantitatively, the  $\text{H}_2\text{O}/\text{Al}$  atom ratio is 1 at 162 °C and substantially decreased to 0.35 and 0.14 at 300 and 450 °C (Figure 5b), respectively. Apparently, the effective desorption of water, with an increase in temperature, was favorable to the recovery of the density of acidic sites.

Further, *in situ* FTIR spectroscopy was utilized to study the evolution of the structure of the  $\text{H}^+(\text{H}_2\text{O})_n$  species and the local environment of the BASs at different temperatures

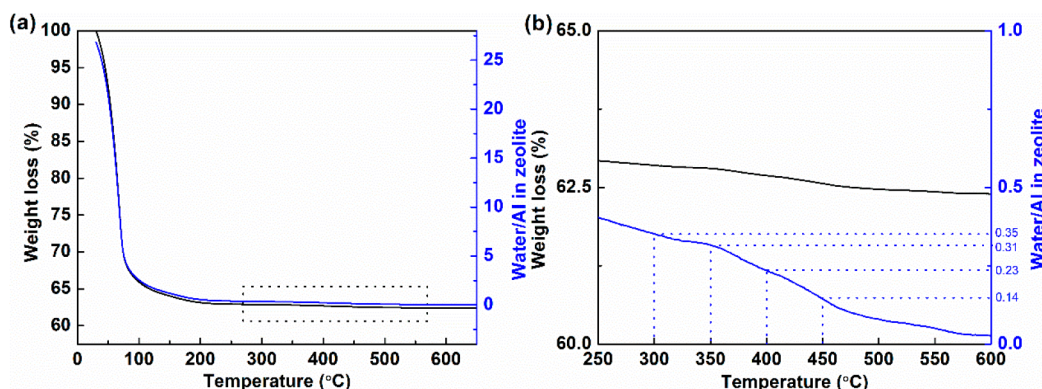


**Figure 5.** Temperature-dependent weight loss (%) (black) of the sample in TGA and the calculated ratio of water molecules to the aluminum atom on H-ZSM-5 (blue): (a) the whole temperature range; (b) the magnified range of 250–600 °C.

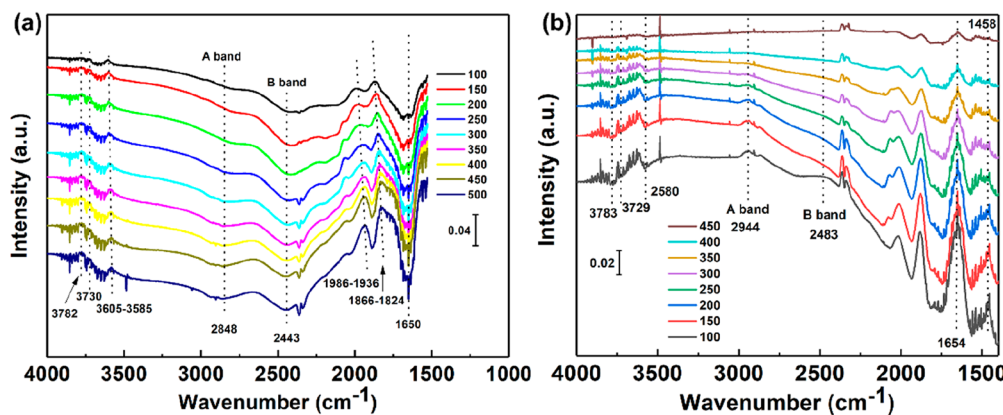


**Figure 6.** *In situ* FTIR spectra of the desorption of water from H-ZSM-5 under vacuum ( $\sim 10^{-5}$  Pa) at different temperatures (a). FTIR spectra of water after subtraction of the H-ZSM-5 500 °C spectrum (b).

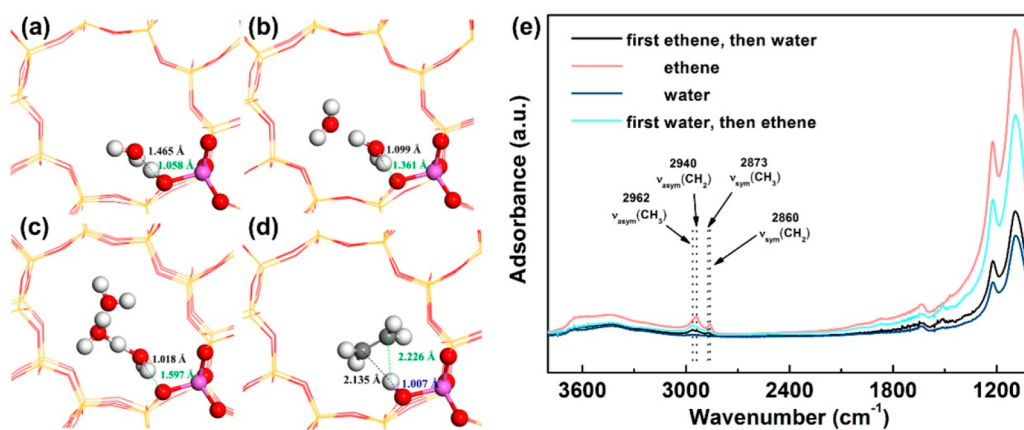


**Figure 7.** Water or ethene adsorption at the T12 BAS of H-ZSM-5: (a) one H<sub>2</sub>O molecule; (b) two H<sub>2</sub>O molecules; (c) three H<sub>2</sub>O molecules; (d) one ethene molecule. (e) IR spectra for ethene and water coadsorption on H-ZSM-5 at 100 °C in two modes: first the adsorption of H<sub>2</sub>O and then ethene or first the adsorption of ethene and then H<sub>2</sub>O.

(Figure 6b). Figure 6a shows the entire FTIR spectra of the hydrated zeolite at different temperatures. Bands pointing upward and downward were associated with increased peak intensity and decreased peak intensity during water desorption, respectively. The peaks at 1986–1936 and 1866–1824 cm<sup>-1</sup> are ascribed to a combination of H-ZSM-5 lattice vibrations.<sup>49,50</sup> An increase in temperature resulted in gradual red shift of these lattice vibration signals.

The peaks at 3782, 3730, and 3605–3585 cm<sup>-1</sup> are ascribed to the terminal silanol groups, the extraframework Al–OH groups, and the bridging structural Si(OH)Al groups, respectively.<sup>51–53</sup> The intensities of these peaks increased gradually with the desorption of water, validating the desorption of water from the acidic sites of the zeolite. In addition, the signal of Si(OH)Al groups is slightly red shifted ( $\sim 20$  cm<sup>-1</sup>) at 500 °C with regard to the signal at 100 °C.

To better illustrate the interaction behavior between water molecules and the acidic sites in the zeolite, the signals of adsorbed water molecules were obtained by subtraction of the H-ZSM-5 500 °C spectrum (Figure 6b). There is an A, B, C triplet of infrared OH bands at  $\sim 2900$ , 2400, and  $\sim 1700$  cm<sup>-1</sup> for Z–OH···H<sub>2</sub>O hydrogen-bonded complexes on zeolites.<sup>54</sup> Owing to the pseudoband nature of A, B, C triplet bands of Z–OH···H<sub>2</sub>O complexes and Fermi resonance,<sup>55,56</sup> the stretching band of the perturbed OH group splits as two peaks located at  $\sim 2600$  and  $\sim 1900$  cm<sup>-1</sup>, respectively. Two peaks at 2944 and

2483 cm<sup>-1</sup> from 100 to 300 °C are assigned to the A and B bands of Z–OH···H<sub>2</sub>O hydrogen-bonded complexes, respectively (Figure 6b). These results all validated the formation of a hydrogen bond of a single H<sub>2</sub>O molecule with a BAS at 100–300 °C.<sup>49</sup> Definitely, the hydrogen bond was destroyed and the peak intensities of A and B bands decreased significantly above 350 °C. The peak at 1458 cm<sup>-1</sup> is attributed to the band of protonated H<sup>+</sup>(H<sub>2</sub>O)<sub>n</sub> species.<sup>57</sup> However, the C band ( $\sim 1700$  cm<sup>-1</sup>) is too weak to be observed, potentially due to the low dosage of adsorbed H<sub>2</sub>O in the sample.<sup>57</sup> In addition, the sharp peak at 1654 cm<sup>-1</sup> is assigned to the deformation vibrations of H<sub>2</sub>O molecules, which were physically adsorbed inside the zeolite.<sup>58</sup> On the basis of these results, we validated the preferential formation of Z–OH···H<sub>2</sub>O hydrogen-bonded complexes and H<sup>+</sup>(H<sub>2</sub>O)<sub>n</sub> species between BASs and adsorbed H<sub>2</sub>O molecules. Apparently, the local environment and properties of BAS changed by H<sub>2</sub>O have a great effect on the adsorption, diffusion, and reactions of other reactants inside the zeolites.

**Competitive Adsorption Behaviors of Ethene and Water on HZSM-5 Catalyst.** Further, periodic DFT calculations were carried out to study the structure of the BASs with or without water. The structure of water inside the cage depends on the number of water molecules (Figure 7a–c). Also, the structure of adsorbed ethene molecules is illustrated in Figure 7d. When a single H<sub>2</sub>O molecule is

adsorbed on the Al T-site (see Figure 7b), water interacts with the hydrogen of the BAS to form a hydrogen bond as a neutral complex, associated with the A, B, C triplet of OH bands in Figure 6a. However, the formation of a strong hydrogen bond between two  $\text{H}_2\text{O}$  molecules and BAS lead to deprotonation and the formation of an  $\text{H}_5\text{O}^+$  hydronium cluster. In addition, a larger hydronium ion cluster is formed by the deprotonation of BASs, absorbing three  $\text{H}_2\text{O}$  molecules. These simulations suggested that the formation of the  $\text{H}_3\text{O}^+(\text{H}_2\text{O})_n$  clusters depends on the number of  $\text{H}_2\text{O}$  molecules ( $\geq 2$ ) adsorbed on BAS, consistent with previous studies.<sup>49,59</sup> As shown in Table S2, the adsorption energies of  $\text{H}_2\text{O}$  and ethene on the BAS are around  $-79$  and  $-71$  kJ/mol, respectively, very close to the data ( $-77$  and  $-67.1$  kJ/mol) in the literature.<sup>60,61</sup> These validated the preferential adsorption of  $\text{H}_2\text{O}$  with BASs during the cofeeding of  $\text{H}_2\text{O}$  with ethene. Actually, a change in the adsorption sequence of water and ethene over H-ZSM-5 at 100 °C was studied with IR (Figure 7e). The bands at 2962, 2940, 2873, and 2860  $\text{cm}^{-1}$  of the adsorbed ethene are assigned to saturated  $\text{CH}_3$  and  $\text{CH}_2$  stretching vibrations.<sup>62</sup> These peaks were the most intense when pure ethene was fed but became very weak when the subsequently adsorbed water removed most of the preadsorbed ethene from the catalyst. In the reverse adsorption sequence, the preadsorbed water occupied most of the BASs, resulting in the weakened adsorption of the subsequently adsorbed ethene, in comparison to that when pure ethene was fed. In summary, there existed two effects: the displacement of the adsorbed ethene by water and the inhibition of ethene by the preadsorbed water. Such a stronger interaction of water with acid sites than with ethene would significantly affect the intrazeolite concentration of adsorbed ethene.

GCMC simulations were applied to identify the preferential adsorption sites of ethene and  $\text{H}_2\text{O}$  molecules in the HMFI framework under the reaction conditions. Red clouds represent the COM (center of mass) density distribution of adsorption sites for  $\text{H}_2\text{O}$  molecules (Figure 8a), validating  $\text{H}_2\text{O}$  molecules in large quantities adsorbed on BASs and the formation of the a water molecular fence (WMF) around BASs at 300 °C. An increase in temperature to 350 °C resulted in the increased density of  $\text{H}_2\text{O}$  adsorbed on other channels and the gradual weakening of the WMF effect around BASs (Figure 8b). Meanwhile, the formation and destruction of  $\text{Z}-\text{OH}\cdots\text{H}_2\text{O}$  hydrogen-bonded complexes and  $\text{H}^+(\text{H}_2\text{O})_n$  species have been observed at 300 and 350 °C, respectively (see Figures S5 and S6). At higher temperature (400–500 °C), the adsorption sites for  $\text{H}_2\text{O}$  molecules were uniformly distributed in the entire framework of HMFI instead of localized around the BASs (see Figure 8c,d and Figure S7). In addition, the simulations of the coexistence of ethene and water suggested that the formed WMF around BASs significantly inhibited the direct access of ethene molecules to the BASs at 300 °C (Figure 8e,h). The WMF was broken at 350 °C or above, due to the desorption of water from BASs (see Figure 8f,g,i,j and Figure S8), resulting in the easy diffusion of ethene through the weakened WMF. Subsequently, ethene was activated by BASs of the zeolite to undergo a further reaction at 350–500 °C.

The olefin-induced HT pathway only depends on the density of BASs, rather than that of the LASs.<sup>63</sup> Therefore, we infer that the adsorption of water on the BASs of catalysts decreases the density of BASs, in turn strongly inhibiting the ethene oligomerization reaction and olefin-induced hydrogen transfer reaction. On the other hand, the alkylation of

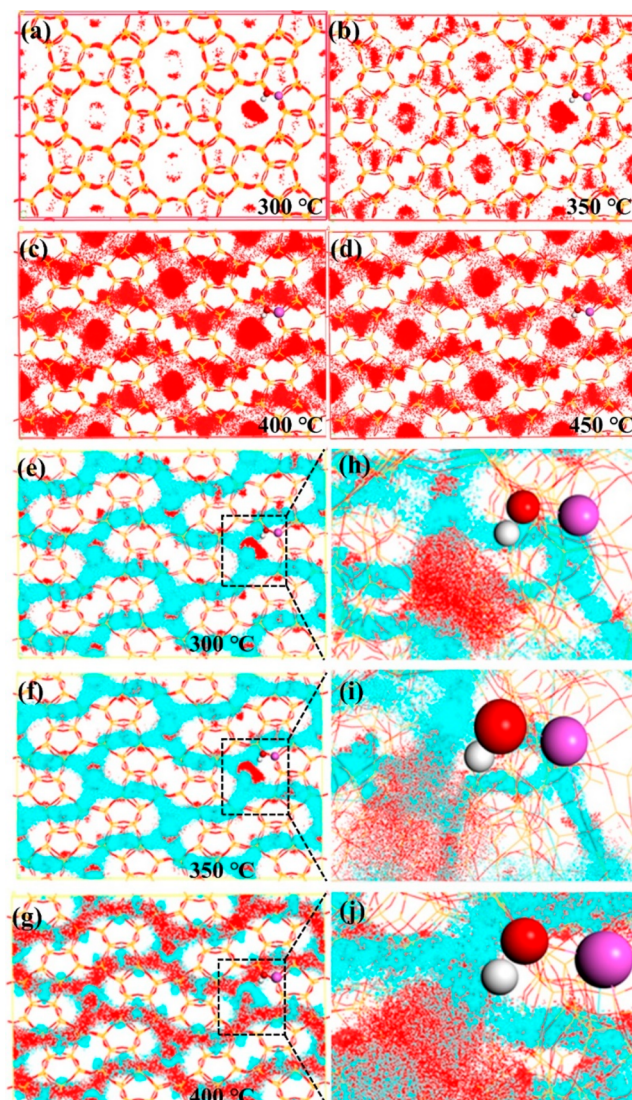


**Figure 8.** Optimized density distribution of adsorption sites of water or ethene molecules in the framework of the HMFI zeolite at different temperatures: (a–d) one-component adsorption process; (e–g) two-component adsorption process. Density distributions around the BASs shown for both ethene and water (h–j). The red and bluish clouds reflect the adsorption probability distribution of water and ethene molecules, respectively. Three water molecules or one ethene molecule were loaded into the framework.

aromatics with ethene is favored mainly due to the accumulation of unreacted ethene. In contrast, the desorption of the majority of adsorbed  $\text{H}_2\text{O}$  molecules on the BAS of catalysts at higher temperatures ( $\geq 350$  °C) dramatically diminishes the concentration of  $\text{Z}-\text{OH}\cdots\text{H}_2\text{O}$  hydrogen-bonded complexes and protonated  $\text{H}^+(\text{H}_2\text{O})_n$  species. Thus, the cofed water has less effect on the BAS concentration as well as the catalytic performance of HZSM-5 in the ETA at high temperatures. Previous work suggested that the characterization of IR and  $^{27}\text{Al}$  MAS NMR gave different decreasing trends in the density of BASs with the addition of water.<sup>64</sup> Overall, the short time (2–3 h) and low temperature (300–500 °C) resulted in a relatively weak dealumination effect of the zeolite sample by steam,<sup>64</sup> as for that in the present work. In addition, the BAS/LAS ratio remained stable at 2.3–2.1 at 2–6 h at 450 °C with a flow rate of steam three times that of

the present work.<sup>64</sup> This is in agreement with the present XRD characterization (see details in Figure S4) and the stable conversion results. However, even the density of BASs changed slightly, the formation of certain bond and WMF effect inside zeolite with water revealed by simulation always effects in a determined temperature. Overall, our experimental data and simulation results provided a deep understanding of the temperature-dependent effect of water, which significantly influenced the conversion rate, the selectivity and yield of hydrocarbon products, and the amount of coke in the zeolite-catalyzed ETA process.

## CONCLUSION

In summary, this work exhibits the influence of water on the heterogeneous catalytic conversion of ethene over H-ZSM-5. At low reaction temperatures ( $\leq 300$  °C), the cofed water preferentially adsorbs on the BASs of the H-ZSM-5 catalysts in comparison with ethene and further leads to the formation of Z—OH···H<sub>2</sub>O hydrogen-bonded complexes and H<sup>+</sup>(H<sub>2</sub>O)<sub>n</sub> species, which results in lower concentrations of ethene within the zeolite as well as consequently lower concentrations of adsorbed reactive intermediates around BASs. Consequently, the oligomerization reaction of ethene, the hydrogen transfer reaction of olefins, and the formation of a hydrocarbon pool within the zeolite channels are significantly suppressed, while the alkylation of aromatics with ethene is enhanced. At higher reaction temperatures ( $\geq 350$  °C), the density of BASs was recovered due to the desorption of the majority of adsorbed H<sub>2</sub>O molecules. Nevertheless, the enhanced confinement effect within zeolites induced by a portion of physically adsorbed water molecules still influences the propagation of the hydrocarbon pool mechanism, exhibiting an overall effect of not changing the conversion of ethene but changing the distribution of aromatics. In addition, the strong interaction of water and BASs and the weakened adsorption of ethene by water were validated with GCMC. The accumulation of larger coke compounds is considerably suppressed by the cofeeding of water and ethene, due to the postponed condensation and polymerization from MAB<sup>+</sup>s to large PAHs. Overall, these results systematically deliver mechanistic insights into the role of water during the ethene conversion process and are helpful in the construction of a more efficient catalytic system for the conversion of oxygen-containing C<sub>1</sub> molecules and biomass.

## ASSOCIATED CONTENT

### Supporting Information

The Supporting Information is available free of charge on the ACS Publications Web site. The Supporting Information is available free of charge at <https://pubs.acs.org/doi/10.1021/acscatal.9b05552>.

Additional catalyst characterization data, GCMC and DFT computational data, and details of the DFT and GCMC computational methods (PDF)

## AUTHOR INFORMATION

### Corresponding Author

Weizhong Qian — Department of Chemical Engineering, Tsinghua University, Beijing 100084, People's Republic of China;  [orcid.org/0000-0002-1684-1061](https://orcid.org/0000-0002-1684-1061); Email: [qianwz@tsinghua.edu.cn](mailto:qianwz@tsinghua.edu.cn)

## Authors

Huiqiu Wang — Department of Chemical Engineering, Tsinghua University, Beijing 100084, People's Republic of China;  [orcid.org/0000-0002-3707-5095](https://orcid.org/0000-0002-3707-5095)

Yilin Hou — Department of Chemical Engineering, Tsinghua University, Beijing 100084, People's Republic of China

Wenjing Sun — School of Chemical Engineering, Sichuan University, Chengdu 610065, Sichuan, People's Republic of China;  [orcid.org/0000-0002-4814-3460](https://orcid.org/0000-0002-4814-3460)

Qikun Hu — Department of Chemical Engineering, Tsinghua University, Beijing 100084, People's Republic of China

Hao Xiong — Department of Chemical Engineering, Tsinghua University, Beijing 100084, People's Republic of China

Tiefeng Wang — Department of Chemical Engineering, Tsinghua University, Beijing 100084, People's Republic of China;  [orcid.org/0000-0002-4607-8650](https://orcid.org/0000-0002-4607-8650)

Binhang Yan — Department of Chemical Engineering, Tsinghua University, Beijing 100084, People's Republic of China

Complete contact information is available at:

<https://pubs.acs.org/10.1021/acscatal.9b05552>

## Notes

The authors declare no competing financial interest.

## ACKNOWLEDGMENTS

The work was financially supported by the National key R&D program of China (2017YFB0602204). The authors are grateful to Tsinghua National Laboratory for Information Science and Technology for assistance with structure simulation.

## REFERENCES

- (1) Olsbye, U.; Svelle, S.; Bjørgen, M.; Beato, P.; Janssens, T. V. W.; Joensen, F.; Bordiga, S.; Lillerud, K. P. Conversion of Methanol to Hydrocarbons: How Zeolite Cavity and Pore Size Controls Product Selectivity. *Angew. Chem., Int. Ed.* **2012**, *51*, 5810–5831.
- (2) Zhou, W.; Cheng, K.; Kang, J.; Zhou, C.; Subramanian, V.; Zhang, Q.; Wang, Y. New Horizon in C1 Chemistry: Breaking the Selectivity Limitation in Transformation of Syngas and Hydrogenation of CO<sub>2</sub> into Hydrocarbon Chemicals and Fuels. *Chem. Soc. Rev.* **2019**, *48* (12), 3193–3228.
- (3) Zhang, J.; Qian, W.; Kong, C.; Wei, F. Increasing Para-Xylene Selectivity in Making Aromatics from Methanol with a Surface-Modified Zn/P/ZSM-5 Catalyst. *ACS Catal.* **2015**, *5* (5), 2982–2988.
- (4) Zhang, H.; Cheng, Y. T.; Vispute, T. P.; Xiao, R.; Huber, G. W. Catalytic Conversion of Biomass-Derived Feedstocks into Olefins and Aromatics with ZSM-5: The Hydrogen to Carbon Effective Ratio. *Energy Environ. Sci.* **2011**, *4* (6), 2297–2307.
- (5) Arslan, M. T.; Qureshi, B. A.; Gilani, S. Z. A.; Cai, D.; Ma, Y.; Usman, M.; Chen, X.; Wang, Y.; Wei, F. Single-Step Conversion of H<sub>2</sub>-Deficient Syngas into High Yield of Tetramethylbenzene. *ACS Catal.* **2019**, *9* (3), 2203–2212.
- (6) Wang, N.; Hou, Y.; Sun, W.; Cai, D.; Chen, Z.; Liu, L.; Ge, B.; Hu, L.; Qian, W.; Wei, F. Modulation of b-Axis Thickness within MFI Zeolite: Correlation with Variation of Product Diffusion and Coke Distribution in the Methanol-to-Hydrocarbons Conversion. *Appl. Catal., B* **2019**, *243*, 721–733.
- (7) Wang, N.; Sun, W.; Hou, Y.; Ge, B.; Hu, L.; Nie, J.; Qian, W.; Wei, F. Crystal-Plane Effects of MFI Zeolite in Catalytic Conversion of Methanol to Hydrocarbons. *J. Catal.* **2018**, *360*, 89–96.
- (8) Wang, N.; Qian, W.; Shen, K.; Su, C.; Wei, F. Bayberry-like ZnO/MFI Zeolite as High Performance Methanol-to-Aromatics Catalyst. *Chem. Commun.* **2016**, *52* (10), 2011–2014.
- (9) Wang, N.; Qian, W.; Wei, F. Fabrication and Catalytic Properties of Three-Dimensional Ordered Zeolite Arrays with Interconnected

- Micro-Meso-Macroporous Structure. *J. Mater. Chem. A* **2016**, *4* (28), 10834–10841.
- (10) Cheng, K.; Zhou, W.; Kang, J.; He, S.; Shi, S.; Zhang, Q.; Pan, Y.; Wen, W.; Wang, Y. Bifunctional Catalysts for One-Step Conversion of Syngas into Aromatics with Excellent Selectivity and Stability. *Chem.* **2017**, *3*, 334–347.
- (11) Zhao, B.; Zhai, P.; Wang, P.; Li, J.; Li, T.; Peng, M.; Zhao, M.; Hu, G.; Yang, Y.; Li, Y.-W.; Zhang, Q.; Fan, W.; Ma, D. Direct Transformation of Syngas to Aromatics over Na-Zn-Fe5C2 and Hierarchical HZSM-5 Tandem Catalysts. *Chem.* **2017**, *3*, 323–333.
- (12) Cui, X.; Gao, P.; Li, S.; Yang, C.; Liu, Z.; Wang, H.; Zhong, L.; Sun, Y. Selective Production of Aromatics Directly from Carbon Dioxide Hydrogenation. *ACS Catal.* **2019**, *9* (5), 3866–3876.
- (13) Olsbye, U.; Svelle, S.; Lillerud, K. P.; Wei, Z. H.; Chen, Y. Y.; Li, J. F.; Wang, J. G.; Fan, W. B. The Formation and Degradation of Active Species during Methanol Conversion over Protonated Zeotype Catalysts. *Chem. Soc. Rev.* **2015**, *44* (20), 7155–7176.
- (14) Wu, X.; Anthony, R. G. Effect of Feed Composition on Methanol Conversion to Light Olefins over SAPO-34. *Appl. Catal., A* **2001**, *218* (1–2), 241–250.
- (15) De Wispelaere, K.; Wondergem, C. S.; Ensing, B.; Hemelsoet, K.; Meijer, E. J.; Weckhuysen, B. M.; Van Speybroeck, V.; Ruiz-Martínez, J. Insight into the Effect of Water on the Methanol-to-Olefins Conversion in H-SAPO-34 from Molecular Simulations and *In Situ* Microspectroscopy. *ACS Catal.* **2016**, *6* (3), 1991–2002.
- (16) Chen, K.; Damron, J.; Pearson, C.; Resasco, D.; Zhang, L.; White, J. L. Zeolite Catalysis: Water Can Dramatically Increase or Suppress Alkane C-H Bond Activation. *ACS Catal.* **2014**, *4* (9), 3039–3044.
- (17) Zhi, Y.; Shi, H.; Mu, L.; Liu, Y.; Mei, D.; Camaiioni, D. M.; Lercher, J. A. Dehydration Pathways of 1-Propanol on HZSM-5 in the Presence and Absence of Water. *J. Am. Chem. Soc.* **2015**, *137* (50), 15781–15794.
- (18) Eckstein, S.; Hintermeier, P. H.; Olarte, M. V.; Liu, Y.; Baráth, E.; Lercher, J. A. Elementary steps and reaction pathways in the aqueous phase alkylation of phenol with ethanol. *J. Catal.* **2017**, *352*, 329–336.
- (19) Liu, Y.; Vjunov, A.; Shi, H.; Eckstein, S.; Camaiioni, D. M.; Mei, D.; Baráth, E.; Lercher, J. A. Enhancing the Catalytic Activity of Hydronium Ions through Constrained Environments. *Nat. Commun.* **2017**, *8*, 14113.
- (20) Liu, Y.; Baráth, E.; Shi, H.; Hu, J.; Camaiioni, D. M.; Lercher, J. A. Solvent-Determined Mechanistic Pathways in Zeolite-H-BEA-Catalysed Phenol Alkylation. *Nat. Catal.* **2018**, *1* (2), 141–147.
- (21) Corma, A. Inorganic Solid Acids and Their Use in Acid-Catalyzed Hydrocarbon Reactions. *Chem. Rev.* **1995**, *95* (3), 559–614.
- (22) Wang, C. M.; Wang, Y. D.; Xie, Z. K. Insights into the Reaction Mechanism of Methanol-to-Olefins Conversion in HSAPO-34 from First Principles: Are Olefins Themselves the Dominating Hydrocarbon Pool Species? *J. Catal.* **2013**, *301*, 8–19.
- (23) Wang, S.; Chen, Y.; Qin, Z.; Zhao, T. S.; Fan, S.; Dong, M.; Li, J.; Fan, W.; Wang, J. Origin and Evolution of the Initial Hydrocarbon Pool Intermediates in the Transition Period for the Conversion of Methanol to Olefins over H-ZSM-5 Zeolite. *J. Catal.* **2019**, *369*, 382–395.
- (24) Van der Borght, K.; Batchu, R.; Galvita, V. V.; Alexopoulos, K.; Reyniers, M. F.; Thybaut, J. W.; Marin, G. B. Insights into the Reaction Mechanism of Ethanol Conversion into Hydrocarbons on H-ZSM-5. *Angew. Chem., Int. Ed.* **2016**, *55* (41), 12817–12821.
- (25) Kresse, G.; Furthmüller, J. Efficient iterative schemes for ab initio total-energy calculations using a plane-wave basis set. *Phys. Rev. B: Condens. Matter Mater. Phys.* **1996**, *54*, 11169–11186.
- (26) Blöchl, P. E. Projector Augmented Wave Method. *Phys. Rev. B: Condens. Matter Mater. Phys.* **1994**, *50*, 17953–17979.
- (27) Perdew, J. P.; Chevary, J. A.; Vosko, S. H.; Jackson, K. A.; Pederson, M. R.; Singh, D. J.; Fiolhais, C. *Phys. Rev. B: Condens. Matter Mater. Phys.* **1992**, *46* (11), 6671–6687.
- (28) Grimme, S.; Antony, J.; Ehrlich, S.; Krieg, H. A Consistent and Accurate ab initio Parametrization of Density Functional Dispersion Correction (DFT-D) for the 94 Elements H-Pu. *J. Chem. Phys.* **2010**, *132* (15), 154104.
- (29) Svelle, S.; Joensen, F.; Nerlov, J.; Olsbye, U.; Lillerud, K. P.; Kolboe, S.; Bjørgen, M. Conversion of Methanol into Hydrocarbons over Zeolite H-ZSM-5: Ethene Formation Is Mechanistically Separated from the Formation of Higher Alkenes. *J. Am. Chem. Soc.* **2006**, *128* (46), 14770–14771.
- (30) Yarulina, I.; Chowdhury, A. D.; Meirer, F.; Weckhuysen, B. M.; Gascon, J. Recent Trends and Fundamental Insights in the Methanol-to-Hydrocarbons Process. *Nat. Catal.* **2018**, *1* (6), 398–411.
- (31) Arslan, M. T.; Ali, B.; Gilani, S. Z. A.; Hou, Y.; Wang, Q.; Cai, D.; Wang, Y.; Wei, F. Selective Conversion of Syngas into Tetramethylbenzene via an Aldol-Aromatic Mechanism. *ACS Catal.* **2020**, *10* (4), 2477–2488.
- (32) Dai, W.; Sun, X.; Tang, B.; Wu, G.; Li, L.; Guan, N.; Hunger, M. Verifying the Mechanism of the Ethene-to-Propene Conversion on Zeolite H-SSZ-13. *J. Catal.* **2014**, *314*, 10–20.
- (33) An, H.; Zhang, F.; Guan, Z.; Liu, X.; Fan, F.; Li, C. Investigating the Coke Formation Mechanism of H-ZSM-5 during Methanol Dehydration Using Operando UV-Raman Spectroscopy. *ACS Catal.* **2018**, *8* (10), 9207–9215.
- (34) Schulz, H. Coking" of Zeolites during Methanol Conversion: Basic Reactions of the MTO-, MTP- and MTG Processes. *Catal. Today* **2010**, *154* (3–4), 183–194.
- (35) Arstad, B.; Nicholas, J. B.; Haw, J. F. Theoretical Study of the Methylbenzene Side-Chain Hydrocarbon Pool Mechanism in Methanol to Olefin Catalysis. *J. Am. Chem. Soc.* **2004**, *126* (9), 2991–3001.
- (36) Goguen, P. W.; Xu, T.; Barich, D. H.; Skloss, T. W.; Song, W.; Wang, Z.; Nicholas, J. B.; Haw, J. F. Pulse-Quench Catalytic Reactor Studies Reveal a Carbon-Pool Mechanism in Methanol-to-Gasoline Chemistry on Zeolite HZSM-5. *J. Am. Chem. Soc.* **1998**, *120* (11), 2650–2651.
- (37) Bjørgen, M.; Bonino, F.; Kolboe, S.; Lillerud, K.; Zecchina, A.; Bordiga, S. Spectroscopic Evidence for a Persistent Benzenium Cation In Zeolite H-Beta. *J. Am. Chem. Soc.* **2003**, *125* (51), 15863–15868.
- (38) McCann, D. M.; Lesthaeghe, D.; Kletnieks, P. W.; Guenther, D. R.; Hayman, M. J.; Van Speybroeck, V.; Waroquier, M.; Haw, J. F. A Complete Catalytic Cycle for Supramolecular Methanol-to-Olefins Conversion by Linking Theory with Experiment. *Angew. Chem., Int. Ed.* **2008**, *47*, 5179–5182.
- (39) Li, J.; Wei, Y.; Chen, J.; Tian, P.; Su, X.; Xu, S.; Qi, Y.; Wang, Q.; Zhou, Y.; He, Y.; Liu, Z. Observation of Heptamethylbenzenium Cation over SAPO-Type Molecular Sieve DNL-6 under Real MTO Conversion Conditions. *J. Am. Chem. Soc.* **2012**, *134* (2), 836–839.
- (40) Xu, S.; Zheng, A.; Wei, Y.; Chen, J.; Li, J.; Chu, Y.; Zhang, M.; Wang, Q.; Zhou, Y.; Wang, J.; Deng, F.; Liu, Z. Direct Observation of Cyclic Carbenium Ions and Their Role in the Catalytic Cycle of the Methanol-to-Olefin Reaction over Chabazite Zeolites. *Angew. Chem., Int. Ed.* **2013**, *52*, 11564–11568.
- (41) Zhang, M.; Xu, S.; Li, J.; Wei, Y.; Gong, Y.; Chu, Y.; Zheng, A.; Wang, J.; Zhang, W.; Wu, X.; et al. Methanol to Hydrocarbons Reaction over H $\beta$  Zeolites Studied by High Resolution Solid-State NMR Spectroscopy: Carbenium Ions Formation and Reaction Mechanism. *J. Catal.* **2016**, *335*, 47–57.
- (42) Zhang, W.; Zhi, Y.; Huang, J.; Wu, X.; Zeng, S.; Xu, S.; Zheng, A.; Wei, Y.; Liu, Z. Methanol to Olefins Reaction Route Based on Methylcyclopentadienes as Critical Intermediates. *ACS Catal.* **2019**, *9* (8), 7373–7379.
- (43) Goetze, J.; Meirer, F.; Yarulina, I.; Gascon, J.; Kapteijn, F.; Ruiz-Martinez, J.; Weckhuysen, B. M. Insights into the Activity and Deactivation of the Methanol-to-Olefins Process over Different Small-Pore Zeolites as Studied with Operando UV-vis Spectroscopy. *ACS Catal.* **2017**, *7* (6), 4033–4046.
- (44) Li, C.; Paris, C.; Martínez-triguero, J.; Boronat, M.; Moliner, M.; Corma, A. Synthesis of Reaction-Adapted Zeolites as Methanol-to-Olefins Catalysts with Mimics of Reaction Intermediates as

- Organic Structure-Directing Agents. *Nat. Catal.* **2018**, *1* (7), 547–554.
- (45) Li, G.; Wang, B.; Resasco, D. E. Water-Mediated Heterogeneously Catalyzed Reactions. *ACS Catal.* **2020**, *10* (2), 1294–1390.
- (46) Haw, J. F.; Song, W.; Marcus, D. M.; Nicholas, J. B. The Mechanism of Methanol to Hydrocarbon Catalysis. *Acc. Chem. Res.* **2003**, *36* (5), 317–326.
- (47) Haw, J. F.; Marcus, D. M. Well-defined (supra) molecular structures in zeolite methanol-to-olefin catalysis. *Top. Catal.* **2005**, *34*, 41–48.
- (48) Allotta, P. M.; Stair, P. C. Time-Resolved Studies of Ethylene and Propylene Reactions in Zeolite H - MFI by In-Situ Fast IR Heating and UV Raman Spectroscopy. *ACS Catal.* **2012**, *2* (11), 2424–2432.
- (49) Vjunov, A.; Wang, M.; Govind, N.; Huthwelker, T.; Shi, H.; Mei, D.; Fulton, J. L.; Lercher, J. A. Tracking the Chemical Transformations at the Brønsted Acid Site upon Water-Induced Deprotonation in a Zeolite Pore. *Chem. Mater.* **2017**, *29* (21), 9030–9042.
- (50) Bernardet, V.; Decrette, A.; Simon, J. M.; Bertrand, O.; Weber, G.; Bellat, J. P. Experimental and Simulated Infrared Spectroscopic Studies of the Interaction of Ethylene on a MFI Zeolite. *Mol. Phys.* **2004**, *102* (16–17), 1859–1870.
- (51) Jacobs, P. A.; Von Ballmoos, R. Framework Hydroxyl Groups of H-ZSM-5 Zeolites. *J. Phys. Chem.* **1982**, *86* (15), 3050–3052.
- (52) Qin, G. On the Framework Hydroxyl Groups of H-ZSM-5 Zeolites. *J. Catal.* **1985**, *95*, 609–612.
- (53) Zholobenko, V. L.; Kustov, L. M.; Borovkov, V. Y.; Kazansky, V. B. A New Type of Acidic Hydroxyl Groups in ZSM-5 Zeolite and in Mordenite According to Diffuse Reflectance i.r. Spectroscopy. *Zeolites* **1988**, *8* (3), 175–178.
- (54) Pelmenschikov, A. G.; Vanwolleput, J.; Janchen, J.; Vansanten, R. A. (A,B,C) Triplet of Infrared OH Bands of Zeolitic H-Complexes. *J. Phys. Chem.* **1995**, *99* (11), 3612–3617.
- (55) Claydon, M. F.; Sheppard, N. The Nature of “A,B,C”-Type Infrared Spectra of Strongly Hydrogen-Bonded Systems; Pseudo-Maxima in Vibrational Spectra. *J. Chem. Soc. D* **1969**, *0*, 1431–1433.
- (56) Evans, J. C. Further Studies of Unusual Effects in the Infrared Spectra of Certain Molecules. *Spectrochim. Acta* **1960**, *16* (9), 994–1000.
- (57) Wakabayashi, F.; Kondo, J. N.; Domen, K.; Hirose, C. FT-IR Study of H<sub>2</sub>18O Adsorption on H-ZSM-5: Direct Evidence for the Hydrogen-Bonded Adsorption of Water. *J. Phys. Chem.* **1996**, *100* (5), 1442–1444.
- (58) Sárkány, J. Effects of Water and Ion-Exchanged Counterion on the FTIR Spectra of ZSM-5. I. NaH-ZSM-5: H-Bonding with OH Groups of Zeolite and Formation of H+(H<sub>2</sub>O)N. *Appl. Catal., A* **1999**, *188* (1–2), 369–379.
- (59) Wang, M.; Jaegers, N. R.; Lee, M. S.; Wan, C.; Hu, J. Z.; Shi, H.; Mei, D.; Burton, S. D.; Camaioni, D. M.; Gutiérrez, O. Y.; et al. Genesis and Stability of Hydronium Ions in Zeolite Channels. *J. Am. Chem. Soc.* **2019**, *141* (8), 3444–3455.
- (60) Mei, D.; Lercher, J. A. Mechanistic Insights into Aqueous Phase Propanol Dehydration in H-ZSM-5 Zeolite. *AIChE J.* **2017**, *63* (1), 172–184.
- (61) Wang, Y.; Wu, B.; Huo, C.; Tao, Z.; Li, Y. A Theoretical Study on the Adsorption of C<sub>2</sub>~6 Olefins on the H-ZSM-5 Zeolite of Periodic Model. *J. Fuel Chem. Technol.* **2014**, *42* (8), 1001–1009.
- (62) Spoto, G.; Bordiga, S.; Ricchiardi, G.; Scarano, D.; Zecchina, A.; Borello, E. IR Study of Ethene and Propene Oligomerization on H-ZSM-5: Hydrogen-Bonded Precursor Formation, Initiation and Propagation Mechanisms and Structure of the Entrapped Oligomers. *J. Chem. Soc., Faraday Trans.* **1994**, *90* (18), 2827–2835.
- (63) Müller, S.; Liu, Y.; Kirchberger, F. M.; Tonigold, M.; Sanchez-Sánchez, M.; Lercher, J. A. Hydrogen Transfer Pathways during Zeolite Catalyzed Methanol Conversion to Hydrocarbons. *J. Am. Chem. Soc.* **2016**, *138* (49), 15994–16003.
- (64) Ong, L. H.; Dömök, M.; Olindo, R.; Van Veen, A. C.; Lercher, J. A. Dealumination of HZSM-5 via Steam-Treatment. *Microporous Mesoporous Mater.* **2012**, *164*, 9–20.